Pergamon

Int. J. Heat Mass Transfer. Vol. 38, No. 7, pp. 1271–1284, 1995

0017-9310/95 $9.50+0.00

0017-9310(94)00236-3

Extension of the continuum model for transport phenomena occurring during metal alloy solidification—I. The conservation equations

J. NI and F. P. INCROPERA†

Heat Transfer Laboratory, School of Mechanical Engineering, Purdue University, West Lafayette, IN 47907, U.S.A.

(*Received* 29 *December* 1993 *and in final form* 19 *July* 1994)

Abstract—In this study, models for simulating transport phenomena occurring during solidification of a binary metal alloy are reviewed, with emphasis placed on the benefits and shortcomings of existing continuum and two-phase approaches. Linkages between the two approaches are discussed, and volume-averaging procedures inherent in the two-phase model are used to develop an extension of the continuum model which retains its computational convenience, while eliminating its inability to treat important features such as solutal undercooling, nucleation, stereological characteristics of the solid/liquid interface, solid movement in the form of floating or settling crystals, and shrinkage. Two approaches to development of a mixture momentum equation are considered, one involving evolution from the liquid momentum conservation equation and the other involving summation of the liquid and solid momentum equations. Special features of both approaches are discussed. In a companion paper, additional models are developed to account for the transport (floating and settling) of solid crystals in the melt, solutal undercooling, and nucleation.

1. INTRODUCTION

Mathematical modeling of transport phenomena associated with the casting of metal alloys is becoming an important tool for determining the state of the final product and for assessing means by which product quality may be improved [2–4]. In addition to determining temperatures and compositions during solidification, modeling has the potential to determine end-state defects such as macrosegregation patterns, void formation, and residual stresses. Since phase change typically occurs over a range of temperatures, a solid/liquid (mushy) zone separates the melt from the fully solidified region, and coupled fluid flows in the mush and the melt may be induced by buoyancy forces, solidification shrinkage, and surface tension gradients, as well as by external forces which may be imposed on the system.

Macrosegregation in the final casting may be influenced by solid movement in a two-phase slurry region, as well as by fluid flow in the mushy zone and the melt. The origins of solid movement can often be traced to heterogeneous nucleation during the early stages of solidification. Heterogeneous nucleation typically occurs on surfaces of the mold walls, yielding stationary, equiaxed crystals which grow quickly and coalesce or are swept into the melt. Crystals which remain attached experience preferential growth parallel, but opposite to, the direction of heat extraction, forming columnar dendrites. Recently, Steube and Hellawell [5] outlined an alternative approach to modeling grain formation in castings, which focused on the production, transport, and survival of crystal fragments. Crystal fragments detached from the mold wall can yield equiaxed grain formation in the bulk liquid. The fragments can also be generated in a developing columnar mushy zone, as ripening within the dendritic structure causes breakage of dendritic sidearms from dendritic stalks. Mushy region flows can transport dendritic fragments into an undercooled region of the melt, where they can grow to form moving equiaxed crystals, or to a region of comparatively large temperature, where they can melt and be reduced to small 'nuclei'. Developing equiaxed crystals may also settle in a gravitational field and accumulate on dendrite tips, thereby precluding further advancement of a columnar dendritic front and initiating a columnar-equiaxed transition (CET). The formation of fragments and transport of equiaxed crystals is schematically illustrated in Fig. 1.

Due to the complexities of dendritic structures, detailed microscopic models which account for transport phenomena in the overall system are beyond the capabilities of today's computing facilities. Hence a macroscopic model must provide the starting point for treating the effects of transport phenomena, while accommodating relevant processes which occur on a microscopic scale [6]. Although most of the recent solidification models have been applied to stationary dendrites, the effect of solid movement on macrosegregation has long been recognized and should be considered in conjunction with an appropriate model

† Author to whom correspondence should be addressed.

NOMENCLATURE

A	area
$\mathbf{B}$	body force per unit mass, or acceleration
B_x	component of $\mathbf{B}$ in the x-coordinate direction of a Cartesian system
c_p	specific heat
C_d	particle drag coefficient
d_s	characteristic diameter of solid crystals
d_2	diameter of secondary dendrite arm
D	mass diffusion tensor of a species in the multi-component mixture
f^α	species concentration of a binary mixture (defined in terms of species mass fraction)
Δf^α	difference between interfacial and volumetric species concentrations
f	mass fraction of solid or liquid phase
$g, \boldsymbol{g}$	volume fraction of solid or liquid phase; gravitational acceleration
h	enthalpy
$\mathbf{k}$	thermal conductivity tensor
$\mathbf{K}$	permeability tensor
L	latent heat of fusion
Le	Lewis number
m_p	slope of liquidus line
$\mathbf{M}$	interfacial momentum transfer rate per unit volume
p	pressure
$\mathbf{R}$	hydraulic resistance tensor
Re	multiphase Reynolds number
S_v	interfacial area concentration
t	time
T	equilibrium temperature
u	x-velocity component in a Cartesian system
$\mathbf{V}$	velocity
V_0	control volume
$\mathbf{W}$	mean growth rate of interface
x	x-coordinate of a Cartesian system
Z	Kozeny coefficient.

Greek symbols

β_c	solutal expansion coefficient
β_t	thermal expansion coefficient
Γ	phase change rate per unit volume
κ_0	permeability coefficient
κ_p	segregation coefficient
μ	dynamic viscosity
ρ	average mass density.

Subscripts

c	solutal
e	eutectic
i	interface
l	liquid phase
ld	liquidus line
m	melting, mixture
0	initial
ref	reference
s	solid phase
sd	solidus line
sol	solidified
sp	solid packing
t	thermal.

Superscripts

d	dissipative
0	reference; previous time
t	transpose tensor
V	per unit volume
α	α species component of a binary alloy
*	effective or macroscopic; prescribed value.

for heterogeneous nucleation. Incorporation of such microscopic solid transport phenomena into a macroscopic description of the casting process is an objective of the next generation of solidification models.

Numerous models have been developed for the solidification of alloys, and comprehensive reviews have recently been published [7–9]. Remarks will therefore be confined to results which bear directly on the objectives of this study. Of particular interest are those models for which the macroscopic conservation equations concurrently apply to the solid, mushy and liquid regions, thereby facilitating use of a single-domain solution with a fixed numerical grid. In one approach [10–14], mixture theory is used to develop a set of mass, momentum, energy, and species conservation equations which may be readily solved with standard numerical procedures [15]. The model has been applied to unidirectional solidification processes and has successfully predicted important phenomena such as diffusive and finger-like double-diffusive convection, irregular liquidus front morphology, remelting, and macrosegregation patterns such as A-segregates, cone segregates and freckles [16–18]. The continuum model was subsequently extended to account for shrinkage-induced convection by considering the density difference between the liquid and solid phases [19].

Although numerical solution of the mixture continuum models is easily implemented by using standard, single-phase CFD procedures, several key assumptions limit their applicability. Solid volume fraction, for example, is obtained either from the lever rule or the Scheil equation, which presume zero macrosegregation. Thermal and solutal nonequilibrium is not treated, and microstructural effects can only be included through formulations for the permeability of the mushy zone. Interfacial species transfer is neglec-

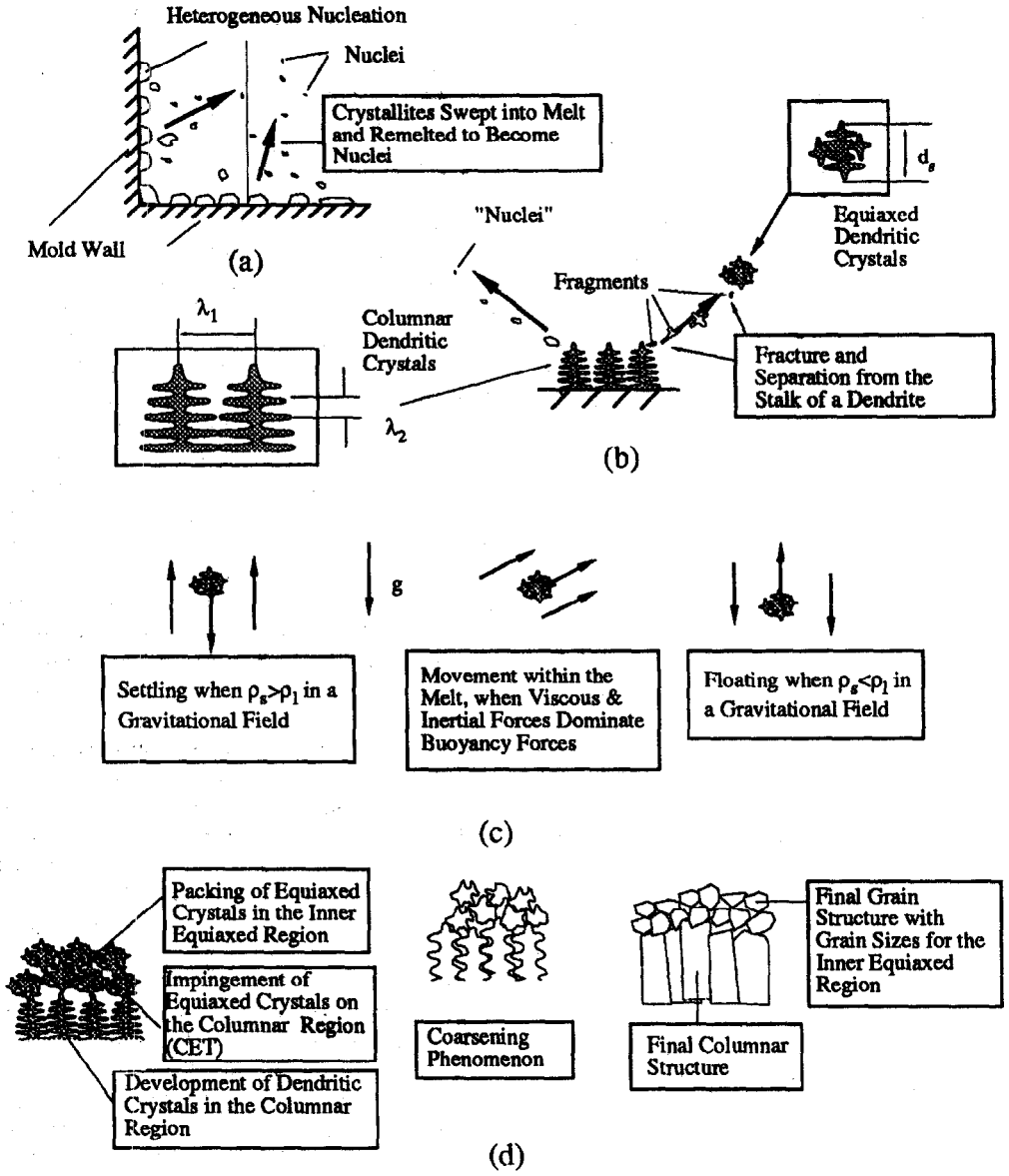

Fig. 1. Schematic illustration of the development and transport of solid structures: (a) heterogeneous nucleation; (b) generation of fragments and equiaxed crystals; (c) transport of solid crystals; (d) packing, impinging, coarsening, and final solid structures.

ted, and either a stationary solid is prescribed or solid movement is considered by postulating *ad hoc* relationships between the liquid and solid velocities. Moreover, specific interfacial geometry and solid structures have not been incorporated into the models, and linkages between physical phenomena occurring on macroscopic and microscopic scales are generally weak.

An alternative approach to the development of macroscopic conservation equations involves use of a volume averaging procedure which can be strongly linked to microscopic conditions. The first usage of this technique in a solidification model was made by Beckermann and Viskanta [20], who considered flow through stationary dendrites in columnar dendritic solidification. Ganesan and Poirier [21] also adopted this technique to derive the mass and momentum equations for flow through a stationary dendritic mushy zone, and Ni and Beckermann [22, 23] used it to develop a two-phase model for solidification of a metal alloy. In the two-phase model, separate volume-averaged mass, momentum, energy and species conservation equations were derived for the solid and liquid phases, thereby permitting a rigorous treatment of disparate solid and liquid velocities, thermal and solutal nonequilibrium, and interfacial momentum, heat and species exchange. Microscopic features can be included through the interfacial transfer terms,

nucleation models, and stereological formulations which account for the geometry of microscopic solid structures [23, 24]. The two-phase model has been applied to columnar dendritic solidification [25] and to equiaxed solidification with liquid convection and solid movement [26, 27].

Although the two-phase model has the potential to concurrently resolve many important micro and macro features of alloy solidification, there are many uncertainties involved in the modeling. Major uncertainties relate to the need for a realistic nucleation model, detailed volumetric heat and mass transfer coefficients (or thermal and solutal diffusion lengths), and correct stereological formulations for interfacial area concentration. A good deal of additional research is needed before the advantages of the model may be fully exploited [8]. In addition, since the model requires the evaluation of many variables, the numerical procedures required to treat physically meaningful systems place a great demand on existing computational capabilities.

Recognizing the benefits and shortcomings of both the continuum and two-phase models, this study has been directed towards extending the capabilities of the continuum model, while continuing to couch the model equations in forms which are amenable to solution by standard numerical procedures. The two-phase formulation of Ni and Beckermann [23] is used to derive a set of continuum mass, momentum, energy, and species conservation equations for which the limiting assumption of negligible solutal undercooling is eliminated, linkages between microscopic and macroscopic phenomena are established, and solid movement is considered.

2. MODEL EQUATIONS

2.1. *Mass conservation*

The volume averaged mass conservation equations for the solid (s) and liquid (l) phases are given by Ni and Beckermann [23]

$$\frac{\partial}{\partial t}(g_l\rho_l)+\nabla\cdot(g_l\rho_l\mathbf{V}_l)=\Gamma_l \tag{1}$$

$$\frac{\partial}{\partial t}(g_s\rho_s)+\nabla\cdot(g_s\rho_s\mathbf{V}_s)=\Gamma_s \tag{2}$$

where g, ρ, $\mathbf{V}$, and Γ refer to the volume fraction, mass-averaged density, volume-averaged velocity vector, and mass transfer rate due to phase change for the respective phases. Summing the equations and applying the interfacial mass balance ($\Gamma_l+\Gamma_s=0$) constraint, the following mixture mass conservation equation may be obtained:

$$\frac{\partial}{\partial t}(\rho_m)+\nabla\cdot(\rho_m\mathbf{V}_m)=0 \tag{3}$$

where the mixture density and velocity are defined as

$$\rho_m=g_l\rho_l+g_s\rho_s \quad \mathbf{V}_m=f_l\mathbf{V}_l+f_s\mathbf{V}_s \tag{4}$$

and the mass fractions f_l and f_s are defined as

$$f_l=\frac{g_l\rho_l}{\rho_m} \quad f_s=\frac{g_s\rho_s}{\rho_m}. \tag{5}$$

2.2. *Momentum conservation*

In the early stages of solidification modeling, the influence of interdendritic convection on macrosegregation was recognized and the mushy region was first treated as a porous medium with Darcy's law used to account for the interdendritic flow [28–34]. Although this law evolved from experimental studies, it can be viewed as a simplified form of the liquid momentum equation for a porous medium [35]. In recent years the liquid momentum equation has been used as the basis of solidification models for which there is no solid movement [20, 21]. Shortcomings of the models relate to (i) their restriction to stationary columnar structures, and (ii) use of an intrinsic liquid velocity as the dependent variable, which precludes expression of the complete set of conservation equations in a form which is convenient for numerical simulation.

Alternatively, Bennon and Incropera [12] used mixture theory to obtain mass, momentum, energy, and species equations which concurrently apply in the melt, mushy and solid regions of a solidification system. Although the model allows for treatment of solid movement, it was cast in a final form which involved a mixture velocity and for which application was restricted to stationary solid structures. However, problematic issues related to the manner in which the Darcy interaction term was included in the mixture momentum equation and linkages which may exist between this equation and the form of the liquid momentum conservation developed for a porous medium. Although Prescott *et al.* [36] addressed these matters in their development of the mixture momentum equation, other issues are in need of clarification. For example, Prescott *et al.* modeled the macroscopic stress of the solid phase by using the solid momentum equation, rather than a constitutive equation, thereby eliminating this momentum equation from further use. Their mixture momentum equation was, in fact, a special form of the liquid momentum equation expressed in terms of a mixture velocity, which precluded rigorous consideration of solid transport. In numerical simulations based on this model, the solid structure was assumed to consist of stationary dendrites ($\mathbf{V}_s=0$), and results should be consistent with those obtained from the liquid momentum equation for a porous medium.

Voller *et al.* [14] and Voller [37] adopted the mixture momentum equation originally developed by Bennon and Incropera [12] and subdivided the mushy region into two zones, one consisting of dispersed solid in a slurry region ($\mathbf{V}_s=\mathbf{V}_l$) and the other consisting of stationary dendrites ($\mathbf{V}_s=0$). The transition between

these two regions was obtained by introducing a consolidation factor which served as the coefficient in a linear relation between liquid and solid velocities. However, their treatment of the consolidation factor lacked a physical basis, and to rigorously establish the solid and liquid velocities, separate solid and liquid momentum conservation equations, or combinations thereof, should be used in lieu of the linear relation.

Relative to recent trends in simulating momentum transfer during alloy solidification, two important criteria for future model development may be identified, namely the need to track solid movement while retaining a set of transport equations amenable to solution by standard numerical procedures. Such a model should include means by which solid and liquid velocities may be rigorously determined and should be couched in terms of a mixture velocity to facilitate the use of standard CFD solution procedures.

Two approaches to treating momentum transfer are considered in the following subsections. In the first approach, evolution of a mixture momentum equation from the liquid momentum equation is addressed. This approach is an adaptation of that traditionally used for porous media, except a mixture velocity is introduced rather than an intrinsic liquid velocity. Alternatively, a mixture solid/liquid momentum model is derived by summing the momentum equations for the solid and liquid phases. Linkages between the approaches, as well as special characteristics of each approach, will also be discussed.

2.2.1. *Liquid momentum model.* Conservation of liquid momentum remains a requirement until a control volume is completely solidified. Hence, as well as being applicable to the liquid region of the solidification system, a liquid momentum equation must also be applicable to fluid motion in a stationary dendritic structure and to the equiaxed solidification of solid crystals in suspension. For a dispersed flow with equiaxed crystal or fragments, the liquid momentum equation may be used with a drag coefficient to model interfacial momentum transfer. In this case, the settling and floating of crystals may be considered to investigate the effect of solid movement on macrosegregation. For a stationary and rigid solid phase, the mushy zone may be viewed as a porous medium, and the effect of interfacial drag may be represented by using Darcy's law (or an extension thereof) with the liquid momentum equation. In this case, the effect of interdendritic flow on macrosegregation can be examined.

Relaxing the requirement of a stationary solid, the liquid momentum equation may be expressed as [23]

$$\begin{aligned}&\frac{\partial}{\partial t}(g_l\rho_l\mathbf{V}_l)+\nabla\cdot(g_l\rho_l\mathbf{V}_l\mathbf{V}_l)\\&\quad=-g_l\nabla p_l+\mathbf{M}_l^d+\mathbf{V}_{li}\Gamma_l+g_l\rho_l\mathbf{B}\\&\qquad+\nabla\cdot\{\mu_l^*\{\nabla(g_l\mathbf{V}_l)+[\nabla(g_l\mathbf{V}_l)]^t\\&\qquad-(\mathbf{V}_{li}:\nabla g_l+\nabla g_l:\mathbf{V}_{li})\}\}.\end{aligned}\tag{6}$$

The effective macroscopic viscosity of the liquid phase μ_l^* accounts for presence of the solid phase and a turbulent stress [23]. However, its determination remains uncertain, and for simplicity it is often taken to be equal to the actual liquid viscosity μ_l. The first and fourth terms on the right-hand side account for the pressure force and additional forces, which may include buoyancy forces and/or externally imposed forces on the liquid phase. In a gravitational field, the body force per unit mass $\mathbf{B}$ is related to the gravitational acceleration vector. If the liquid density varies with temperature and/or solutal concentration, Boussinesq's approximation can be adopted to express the buoyancy force in terms of thermal and solutal expansion coefficients. The fourth term on the right side of equation (6) then reduces to $g_l\rho_l[\beta_t(T-T_{ref})+\beta_c(f_l^a-f_{l\,ref}^a)]$, where β_t and β_c are the thermal and solutal expansion coefficients and T and f_l^a are the local liquid temperature and species concentration.

If the mixture velocity defined by equation (4) is selected as the dependent variable, the first term on the left-hand side of equation (6) can be expressed as

$$\frac{\partial}{\partial t}(g_l\rho_l\mathbf{V}_l)=\frac{\partial}{\partial t}(\rho_m\mathbf{V}_m)-\frac{\partial}{\partial t}(g_s\rho_s\mathbf{V}_s)\tag{7}$$

and the second term, the liquid advection term, can be expressed as

$$\begin{aligned}\nabla\cdot(g_l\rho_l\mathbf{V}_l\mathbf{V}_l)&=\nabla\cdot(\rho_m\mathbf{V}_m\mathbf{V}_m)+\nabla\\&\quad\cdot(g_l\rho_l\mathbf{V}_l\mathbf{V}_l-\rho_m\mathbf{V}_m\mathbf{V}_m)\\&=\nabla\cdot(\rho_m\mathbf{V}_m\mathbf{V}_m)+\nabla\\&\quad\cdot\left[\left(\frac{\rho_m f_s}{f_l}\right)(\mathbf{V}_m-\mathbf{V}_s)(\mathbf{V}_m-\mathbf{V}_s)\right]\\&\quad-\nabla\cdot(g_s\rho_s\mathbf{V}_s\mathbf{V}_s).\end{aligned}\tag{8}$$

The third term on the right-hand side of equation (6) represents interfacial momentum transfer due to phase change, and it has been expressed in terms of the product of the phase change rate per unit volume and the liquid interfacial velocity. The liquid and solid interfacial velocities can be expressed in terms of an absolute interface velocity and a mean growth rate due to phase change at the solid/liquid interface [38]. That is,

$$\mathbf{V}_{li}=\mathbf{V}_i+\mathbf{W}_l\quad\text{and}\quad\mathbf{V}_{si}=\mathbf{V}_i+\mathbf{W}_s\tag{9}$$

where the mean growth rates of the liquid and solid phases, $\mathbf{W}_l$ and $\mathbf{W}_s$, can be calculated through incorporation of a kinetic law for the growth and formation of microstructures. Alternatively, they can be expressed as [38]

$$\mathbf{W}_l=\frac{\Gamma_l}{S_v^2\rho_l}\nabla g_l\quad\text{and}\quad\mathbf{W}_s=\frac{\Gamma_s}{S_v^2\rho_s}\nabla g_s.\tag{10}$$

Thus, with $\nabla g_l=-\nabla g_s$ and $\Gamma_l=-\Gamma_s$, the liquid interfacial velocity can be expressed as [23]

$$\mathbf{V}_{\mathrm{li}} = \mathbf{V}_{\mathrm{si}} - \frac{(\rho_{\mathrm{l}} - \rho_{\mathrm{s}})\,\Gamma_{\mathrm{s}}}{\rho_{\mathrm{s}}\rho_{\mathrm{l}} S_{\mathrm{v}}^2}\nabla g_{\mathrm{s}}. \tag{11}$$

The interfacial area concentration, S_{v}, is defined as the total solid/liquid interfacial area within a control volume (A_{i}/V_0) and is used to characterize first-order geometric effects. In general, it is a function of the solid volume fraction and solid/liquid interface geometry, and appropriate expressions may be formulated through stereological descriptions of the interface. For translational motion of rigid solid crystals, it is reasonable to assume that

$$\mathbf{V}_{\mathrm{si}} = \mathbf{V}_{\mathrm{s}}. \tag{12}$$

With equation (11), the model for interfacial momentum transfer due to phase change accounts for the influence of density differences between the solid and liquid phases. The effect may become important under conditions for which shrinkage induced flow is significant. For example, in the absence of other mechanisms for sustaining liquid flow, once solidification begins with $\rho_{\mathrm{s}} > \rho_{\mathrm{l}}$, the third term on the right-hand side of equation (6) provides the driving force for shrinkage-induced liquid flow. The direction of the induced flow opposes that of the solidification direction, and its magnitude depends on the density difference, interfacial area concentration, gradient of the solid volume fraction, and the phase change rate.

The fifth term on the right-hand side of equation (6) is the total liquid macroscopic viscous stress, which can also be expressed as

$$\begin{aligned}
&\nabla\cdot\{\mu_{\mathrm{l}}^*\{\nabla(g_{\mathrm{l}}\mathbf{V}_{\mathrm{l}}) + [\nabla(g_{\mathrm{l}}\mathbf{V}_{\mathrm{l}})]^{\mathrm{t}} \\
&\quad -(\mathbf{V}_{\mathrm{li}}:\nabla g_{\mathrm{l}} + \nabla g_{\mathrm{l}}:\mathbf{V}_{\mathrm{li}})\}\} \\
&= \nabla\cdot\left\{\mu_{\mathrm{l}}^*\left\{\nabla\left(\frac{\rho_{\mathrm{m}}\mathbf{V}_{\mathrm{m}}}{\rho_{\mathrm{l}}}\right) + \left[\nabla\left(\frac{\rho_{\mathrm{m}}\mathbf{V}_{\mathrm{m}}}{\rho_{\mathrm{l}}}\right)\right]^{\mathrm{t}}\right\}\right\} \\
&\quad -\nabla\cdot\left\{\mu_{\mathrm{l}}^*\left\{\nabla\left(\frac{\rho_{\mathrm{m}} f_{\mathrm{s}}\mathbf{V}_{\mathrm{s}}}{\rho_{\mathrm{l}}}\right) + \left[\nabla\left(\frac{\rho_{\mathrm{m}} f_{\mathrm{s}}\mathbf{V}_{\mathrm{s}}}{\rho_{\mathrm{l}}}\right)\right]^{\mathrm{t}}\right\}\right\} \\
&\quad -\nabla\cdot\{\mu_{\mathrm{l}}^*\{\mathbf{V}_{\mathrm{li}}:\nabla g_{\mathrm{l}} + \nabla g_{\mathrm{l}}:\mathbf{V}_{\mathrm{li}}\}\} \\
&= \nabla\cdot\left\{\mu_{\mathrm{l}}^*\frac{\rho_{\mathrm{m}}}{\rho_{\mathrm{l}}}[\nabla\mathbf{V}_{\mathrm{m}} + (\nabla\mathbf{V}_{\mathrm{m}})^{\mathrm{t}}]\right\} \\
&\quad +\nabla\cdot\left\{\mu_{\mathrm{l}}^*\left[\mathbf{V}_{\mathrm{m}}:\nabla\left(\frac{\rho_{\mathrm{m}}}{\rho_{\mathrm{l}}}\right) + \nabla\left(\frac{\rho_{\mathrm{m}}}{\rho_{\mathrm{l}}}\right):\mathbf{V}_{\mathrm{m}}\right]\right\} \\
&\quad -\nabla\cdot\left\{\mu_{\mathrm{l}}^*\frac{\rho_{\mathrm{m}} f_{\mathrm{s}}}{\rho_{\mathrm{l}}}[\nabla\mathbf{V}_{\mathrm{s}} + (\nabla\mathbf{V}_{\mathrm{s}})^{\mathrm{t}}]\right\} \\
&\quad -\nabla\cdot\left\{\mu_{\mathrm{l}}^*\left[\mathbf{V}_{\mathrm{s}}:\left(\nabla\frac{\rho_{\mathrm{m}} f_{\mathrm{s}}}{\rho_{\mathrm{l}}}\right) + \left(\nabla\frac{\rho_{\mathrm{m}} f_{\mathrm{s}}}{\rho_{\mathrm{l}}}\right):\mathbf{V}_{\mathrm{s}}\right]\right\} \\
&\quad +\nabla\cdot\{\mu_{\mathrm{l}}^*\{\mathbf{V}_{\mathrm{li}}:\nabla g_{\mathrm{s}} + \nabla g_{\mathrm{s}}:\mathbf{V}_{\mathrm{li}}\}\}.
\end{aligned} \tag{13}$$

The first term on the right-hand side of equation (13) is the standard viscous stress, while the second term accounts for the effect of solid and/or liquid phase density changes on the total macroscopic viscous stress. The fifth term on the right-hand side of equation (13) accounts for the contribution of interface motion to the liquid viscous stress [23, 38]. The third and fourth terms account for solid movement and vanish for the limiting case of stationary dendrites. In this limit the first and second terms reduce to the standard form of the macroscopic stress for a liquid phase. In the limit of equivalent phase densities, the second term vanishes, $V_{\mathrm{li}} = V_{\mathrm{s}}$ [see equation (11)], and the fourth and fifth terms cancel, while the first and third terms reduce to standard forms of the liquid and solid viscous stresses. Note that the second and fourth terms do not provide driving forces for flow induced by density changes (that is, shrinkage induced flow), but simply represent contributions to the total macroscopic stress due to density differences between the solid and liquid phases.

The second term on the right-hand side of equation (6) represents momentum transfer due to interfacial interactions between the liquid and solid phases. This term is proportional to the difference between the intrinsic volume-averaged velocities of the solid and liquid and may be expressed as [23]

$$\mathbf{M}_{\mathrm{l}}^{\mathrm{d}} = -\mathbf{R}:(\mathbf{V}_{\mathrm{l}} - \mathbf{V}_{\mathrm{s}}) = -\frac{\mathbf{R}\rho_{\mathrm{m}}}{g_{\mathrm{l}}\rho_{\mathrm{l}}}:(\mathbf{V}_{\mathrm{m}} - \mathbf{V}_{\mathrm{s}}) \tag{14}$$

where $\mathbf{R}$ is a hydraulic resistance tensor. Generalized mathematical models for the tensor are provided by Ni and Beckermann [23].

Momentum transfer due to interfacial interactions between the liquid and solid phases may be expressed in terms of a drag coefficient for the movement of equiaxed crystals in the melt [39]. That is,

$$\begin{aligned}
\mathbf{M}_{\mathrm{l}}^{\mathrm{d}} &= \frac{3}{4d_{\mathrm{s}}} g_{\mathrm{s}}\rho_{\mathrm{l}} C_{\mathrm{d}} |\mathbf{V}_{\mathrm{s}} - \mathbf{V}_{\mathrm{l}}| (\mathbf{V}_{\mathrm{s}} - \mathbf{V}_{\mathrm{l}}) \\
&= -\frac{3}{4d_{\mathrm{s}}}\frac{g_{\mathrm{s}}}{g_{\mathrm{l}}}\rho_{\mathrm{m}} C_{\mathrm{d}} |\mathbf{V}_{\mathrm{s}} - \mathbf{V}_{\mathrm{l}}| (\mathbf{V}_{\mathrm{m}} - \mathbf{V}_{\mathrm{s}})
\end{aligned} \tag{15}$$

where d_{s} is a characteristic diameter of the solid crystals. The drag coefficient C_{d} may be expressed in terms of a multiphase Reynolds number,

$$C_{\mathrm{d}} = \frac{24}{Re_{\mathrm{m}}} \quad \text{and} \quad Re_{\mathrm{m}} = \frac{\rho_{\mathrm{l}} |\mathbf{V}_{\mathrm{s}} - \mathbf{V}_{\mathrm{l}}| d_{\mathrm{s}}}{\mu_{\mathrm{m}}} \tag{16}$$

where μ_{m} is the mixture viscosity. From rheological considerations, the mixture viscosity can be expressed as [39]

$$\mu_{\mathrm{m}} = \left(1 - \frac{g_{\mathrm{s}}}{g_{\mathrm{sp}}}\right)^{-2.5 g_{\mathrm{sp}}} \mu_{\mathrm{l}} \tag{17}$$

where g_{sp} is the maximum packing fraction of the solid phase.

Momentum transfer due to interfacial interactions between the liquid and solid phases may also be expressed in terms of a permeability tensor for flow through a continuous solid structure such as columnar dendritic arrays. In particular,

$$\mathbf{M}_{\mathrm{l}}^{\mathrm{d}} = -g_{\mathrm{l}}\frac{\rho_{\mathrm{m}}\mu_{\mathrm{l}}}{\rho_{\mathrm{l}}}\mathbf{K}^{-1}:(\mathbf{V}_{\mathrm{m}} - \mathbf{V}_{\mathrm{s}}) \tag{18}$$

where $\mathbf{K}$ is the permeability tensor of an anisotropic dendritic structure.

Although rigorous models of the permeability components for anisotropic solid structures are lacking, experimental data are available [40, 41]. In most simulations, the solid structures (equiaxed crystals or columnar dendrites) are usually assumed to be isotropic, and the Kozeny–Carman expression may be utilized to express the permeability as $g_l^3 d_s^2/[Z(1-g_l)^2]$ or $\kappa_0 g_l^3/(1-g_l)^2$, where Z, d_s and κ_0 are the Kozeny coefficient, a characteristic length of the solid structure, and the permeability coefficient, respectively.

Substituting from equations (7), (8), (13) and (14), the mixture momentum conservation equation, equation (6), can be expressed as

$$\begin{aligned}
&\frac{\partial}{\partial t}(\rho_m \mathbf{V}_m)+\nabla\cdot(\rho_m \mathbf{V}_m \mathbf{V}_m)\\
&= -g_l\nabla p_l - \frac{\mathbf{R}\rho_m}{g_l\rho_l}:(\mathbf{V}_m-\mathbf{V}_s)+\mathbf{V}_{li}\Gamma_l\\
&\quad +g_l\rho_l\mathbf{B}-\nabla\cdot\left[\left(\frac{\rho_m f_s}{f_l}\right)(\mathbf{V}_m-\mathbf{V}_s)(\mathbf{V}_m-\mathbf{V}_s)\right]\\
&\quad +\frac{\partial}{\partial t}(g_s\rho_s\mathbf{V}_s)+\nabla\cdot(g_s\rho_s\mathbf{V}_s\mathbf{V}_s)\\
&\quad +\nabla\cdot\left\{\mu_l^*\frac{\rho_m}{\rho_l}[\nabla\mathbf{V}_m+(\nabla\mathbf{V}_m)^t]\right\}\\
&\quad +\nabla\cdot\left\{\mu_l^*\left[\mathbf{V}_m:\nabla\left(\frac{\rho_m}{\rho_l}\right)+\nabla\left(\frac{\rho_m}{\rho_l}\right):\mathbf{V}_m\right]\right\}\\
&\quad -\nabla\cdot\left\{\mu_l^*\frac{\rho_m f_s}{\rho_l}[\nabla\mathbf{V}_s+(\nabla\mathbf{V}_s)^t]\right\}\\
&\quad -\nabla\cdot\left\{\mu_l^*\left[\mathbf{V}_s:\left(\nabla\frac{\rho_m f_s}{\rho_l}\right)+\left(\nabla\frac{\rho_m f_s}{\rho_l}\right):\mathbf{V}_s\right]\right\}\\
&\quad +\nabla\cdot\{\mu_l^*[\mathbf{V}_{li}:(\nabla g_s)+(\nabla g_s):\mathbf{V}_{li}]\}. \qquad (19)
\end{aligned}$$

For the x-coordinate direction of a Cartesian system, the equation becomes

$$\begin{aligned}
&\frac{\partial}{\partial t}(\rho_m u_m)+\nabla\cdot(\rho_m \mathbf{V}_m u_m)\\
&= -g_l\frac{\partial p_l}{\partial x}-\frac{R_x\rho_m}{g_l\rho_l}(u_m-u_s)+u_{li}\Gamma_l\\
&\quad +g_l\rho_l B_x-\nabla\cdot\left[\left(\frac{\rho_m f_s}{f_l}\right)(\mathbf{V}_m-\mathbf{V}_s)(u_m-u_s)\right]\\
&\quad +\frac{\partial}{\partial t}(g_s\rho_s u_s)+\nabla\cdot(g_s\rho_s\mathbf{V}_s u_s)\\
&\quad +\nabla\cdot\left(\mu_l^*\frac{\rho_m}{\rho_l}\nabla u_m\right)+\nabla\cdot\left[\mu_l^* u_m\nabla\left(\frac{\rho_m}{\rho_l}\right)\right]\\
&\quad -\nabla\cdot\left(\mu_l^*\frac{\rho_m f_s}{\rho_l}\nabla u_s\right)-\nabla\cdot\left[\mu_l^* u_s\nabla\left(\frac{\rho_m f_s}{\rho_l}\right)\right]\\
&\quad +\nabla\cdot[\mu_l^* u_{li}(\nabla g_s)] \qquad (20)
\end{aligned}$$

where u_m is the mixture velocity component in the x direction.

2.2.2. *Mixture momentum model.* In an alternative approach, one may apply the Navier–Stokes equations to both the liquid and solid phases, with the solid treated as a pseudo-fluid, and the equations may be summed to obtain a mixture momentum equation. Such an approach has been successfully applied to multi-particulate systems, such as a suspended particulate flow or a fluidized bed [42]. However, for stationary solids such as columnar dendrites attached to a mold wall or packed equiaxed crystals, the solid may not be treated as a pseudo-fluid and the solid transport momentum equation is no longer valid. Nevertheless, since the solid is stationary, the liquid equation governs momentum transport for the mixture and the interdendritic flow can be treated as liquid flow through a porous medium. However, a critical issue relates to the transition from a suspended particulate system to a packed bed or otherwise stationary solid. Complicating features include the non-Newtonian rheological behavior of a dense solid suspension, the dynamics of solid particle impingement and adhesion, and force interactions with system boundaries. To accommodate the transition to zero-velocity of the solid phase when a slurry of suspended particles agglomerates or attaches to a dendritic front, one needs a mathematical model which can account for solid crystal movement and convert this movement to a stationary state.

The solid momentum equation can be expressed as [23]

$$\begin{aligned}
&\frac{\partial}{\partial t}(g_s\rho_s\mathbf{V}_s)+\nabla\cdot(g_s\rho_s\mathbf{V}_s\mathbf{V}_s)\\
&\quad = -g_s\nabla p_s+\mathbf{M}_s^d+\mathbf{V}_{si}\Gamma_s+g_s\rho_s\mathbf{B}\\
&\qquad +\nabla\cdot\{\mu_s^*\{\nabla(g_s\mathbf{V}_s)+[\nabla(g_s\mathbf{V}_s)]^t\\
&\qquad -(\mathbf{V}_{si}:\nabla g_s+\nabla g_s:\mathbf{V}_{si})\}\}\\
&\quad = -g_s\nabla p_s+\mathbf{M}_s^d+\mathbf{V}_s\Gamma_s+g_s\rho_s\mathbf{B}\\
&\qquad +\nabla\cdot\{g_s\mu_s^*[\mathbf{V}_s+(\nabla\mathbf{V}_s)^t]\} \qquad (21)
\end{aligned}$$

where $\mathbf{V}_{si}$ has been replaced by $\mathbf{V}_s$ from equation (12). A mixture momentum equation can be obtained by summing momentum equations for the liquid and solid phases, equations (6) and (21), and utilizing an interfacial momentum balance of the form [23], $\mathbf{V}_{li}\Gamma_l+\mathbf{V}_{si}\Gamma_s+\mathbf{M}_l^d+\mathbf{M}_s^d=0$, to yield

$$\begin{aligned}
&\frac{\partial}{\partial t}(\rho_m\mathbf{V}_m)+\nabla\cdot(\rho_m\mathbf{V}_m\mathbf{V}_m)\\
&\quad = -g_l\nabla p_l-g_s\nabla p_s+\rho_m\mathbf{B}-\nabla\\
&\qquad \cdot\left[\left(\frac{\rho_m f_s}{f_l}\right)(\mathbf{V}_m-\mathbf{V}_s)(\mathbf{V}_m-\mathbf{V}_s)\right]\\
&\qquad +\nabla\cdot\left\{\mu_l^*\frac{\rho_m}{\rho_l}[\nabla\mathbf{V}_m+(\nabla\mathbf{V}_m)^t]\right\}+\nabla
\end{aligned}$$

$$\cdot\left\{\mu_l^*\left[\mathbf{V}_m:\nabla\left(\frac{\rho_m}{\rho_l}\right)+\nabla\left(\frac{\rho_m}{\rho_l}\right):\mathbf{V}_m\right]\right\}-\nabla$$
$$\cdot\left\{\mu_l^*\frac{\rho_m f_s}{\rho_l}[\nabla\mathbf{V}_s+(\nabla\mathbf{V}_s)^t]\right\}-\nabla$$
$$\cdot\left\{\mu_l^*\left[\mathbf{V}_s:\left(\nabla\frac{\rho_m f_s}{\rho_l}\right)+\left(\nabla\frac{\rho_m f_s}{\rho_l}\right):\mathbf{V}_s\right]\right\}$$
$$+\nabla\cdot\{\mu_l^*[\mathbf{V}_{li}:(\nabla g_s)+(\nabla g_s):\mathbf{V}_{li}]\}+\nabla$$
$$\cdot\{g_s\mu_s^*[\nabla\mathbf{V}_s+(\nabla\mathbf{V}_s)^t]\}. \quad (22)$$

The result is similar to equation (19), except that (i) the interfacial momentum transfer terms are absent, (ii) there is a pressure gradient term for the solid phase, (iii) the buoyancy force is expressed in terms of the mixture density, (iv) solid transient and advection momentum transport terms are absent on the right-hand side of equation (22), and (v) a macroscopic solid viscous stress appears as the tenth term on the right-hand side of equation (22). The solid macroscopic viscous stress has been expressed in terms of the derivative of the solid velocity and an effective solid viscosity, μ_s^*, which, from the rheology of suspensions, can be modeled as [27]

$$\mu_s^*=\frac{\mu_m-(1-g_s)\mu_l^*}{g_s}=\frac{\left(1-\dfrac{g_s}{g_{sp}}\right)^{-2.5g_{sp}}-1+g_s}{g_s}\mu_l^*. \quad (23)$$

Equation (22) may be simplified for a dispersed flow of crystals and for a system of stationary dendrites.

2.2.2(a). Dispersed flow with moving equiaxed crystals. For a dispersed flow with moving equiaxed crystals, mechanical equilibrium may be assumed [43], in which case $p_s = p_l = p$, where p is the equilibrium pressure. The mixture momentum equation (22) then reduces to

$$\frac{\partial}{\partial t}(\rho_m\mathbf{V}_m)+\nabla\cdot(\rho_m\mathbf{V}_m\mathbf{V}_m)$$
$$=-\nabla p+\rho_m\mathbf{B}-\nabla\cdot\left[\left(\frac{\rho_m f_s}{f_l}\right)(\mathbf{V}_m-\mathbf{V}_s)(\mathbf{V}_m-\mathbf{V}_s)\right]$$
$$+\nabla\cdot\left\{\mu_l^*\frac{\rho_m}{\rho_l}[\nabla\mathbf{V}_m+(\nabla\mathbf{V}_m)^t]\right\}+\nabla$$
$$\cdot\left\{\mu_l^*\left[\mathbf{V}_m:\nabla\left(\frac{\rho_m}{\rho_l}\right)+\nabla\left(\frac{\rho_m}{\rho_l}\right):\mathbf{V}_m\right]\right\}$$
$$-\nabla\cdot\left\{\mu_l^*\frac{\rho_m f_s}{\rho_l}[\nabla\mathbf{V}_s+(\nabla\mathbf{V}_s)^t]\right\}-\nabla$$
$$\cdot\left\{\mu_l^*\left[\mathbf{V}_s:\left(\nabla\frac{\rho_m f_s}{\rho_l}\right)+\left(\nabla\frac{\rho_m f_s}{\rho_l}\right):\mathbf{V}_s\right]\right\}$$
$$+\nabla\cdot\{\mu_l^*[\mathbf{V}_{li}:(\nabla g_s)+(\nabla g_s):\mathbf{V}_{li}]\}$$
$$+\nabla\cdot\{g_s\mu_s^*[\nabla\mathbf{V}_s+(\nabla\mathbf{V}_s)^t]\}. \quad (24)$$

In the x-coordinate direction of a Cartesian system, the equation can be expressed as

$$\frac{\partial}{\partial t}(\rho_m u_m)+\nabla\cdot(\rho_m\mathbf{V}_m u_m)=$$
$$-\frac{\partial p}{\partial x}+\rho_m B_x-\nabla\cdot\left[\left(\frac{\rho_m f_s}{f_l}\right)(\mathbf{V}_m-\mathbf{V}_s)(u_m-u_s)\right]+\nabla$$
$$\cdot\left(\mu_l^*\frac{\rho_m}{\rho_l}\nabla u_m\right)+\nabla\cdot\left[\mu_l^* u_m\nabla\left(\frac{\rho_m}{\rho_l}\right)\right]-\nabla$$
$$\cdot\left(\mu_l^*\frac{\rho_m f_s}{\rho_l}\nabla u_s\right)-\nabla\cdot\left[\mu_l^* u_s\nabla\left(\frac{\rho_m f_s}{\rho_l}\right)\right]+\nabla$$
$$\cdot[\mu_l^* u_{li}(\nabla g_s)]+\nabla\cdot[g_s\mu_s^*\nabla u_s]. \quad (25)$$

2.2.2(b). Stationary mushy zone. When the solid structure is stationary, the solid phase cannot be treated as a pseudo-fluid and the pressure and stress imposed by the liquid phase at the solid/liquid interface can be transferred through the solid phase. Hence, there is a pressure field within the solid phase, which must be balanced with the interfacial momentum transfer if forces are assumed not to be transferred to the mold wall through the solid and deformation of the solid is neglected. From specialization of the solid momentum equation, equation (21), for zero velocity of the solid phase, it follows that

$$-g_s\nabla p_s+\mathbf{M}_s^d+\mathbf{V}_{si}\Gamma_s+g_s\rho_s\mathbf{B}=0. \quad (26)$$

Obtaining the solid pressure gradient from the above relation and introducing the interfacial momentum balance, $\mathbf{V}_{si}\Gamma_s+\mathbf{M}_s^d=-\mathbf{M}_l^d-\mathbf{V}_{li}\Gamma_l$, the mixture momentum equation, equation (22), for zero solid movement ($\mathbf{V}_s=0$) becomes

$$\frac{\partial}{\partial t}(\rho_m\mathbf{V}_m)+\nabla\cdot(\rho_m\mathbf{V}_m\mathbf{V}_m)$$
$$=-g_l\nabla p_l-\frac{\mathbf{R}\rho_m}{g_l\rho_l}:\mathbf{V}_m+V_{li}\Gamma_l$$
$$+g_l\rho_l\mathbf{B}-\nabla\cdot\left[\left(\frac{\rho_m f_s}{f_l}\right)\mathbf{V}_m\mathbf{V}_m\right]+\nabla$$
$$\cdot\left\{\mu_l^*\frac{\rho_m}{\rho_l}[\nabla\mathbf{V}_m+(\nabla\mathbf{V}_m)^t]\right\}+\nabla$$
$$\cdot\left\{\mu_l^*\left[\mathbf{V}_m:\nabla\left(\frac{\rho_m}{\rho_l}\right)+\nabla\left(\frac{\rho_m}{\rho_l}\right):\mathbf{V}_m\right]\right\}+\nabla$$
$$\cdot\{\mu_l^*[\mathbf{V}_{li}:(\nabla g_s)+(\nabla g_s):\mathbf{V}_{li}]\} \quad (27)$$

where, in this case, $V_{li}=-(\rho_l-\rho_s)\Gamma_s/(\rho_s\rho_l S_v^2)\nabla g_s$ and $V_{si}=V_s=0$.

Although a summation procedure involving the solid and liquid momentum equations was used, the mixture momentum equation contains the liquid interfacial momentum transfer terms. Interfacial interactions manifested by the second term on the right-hand side of equation (27) may be modeled by equation (18) and hence through use of a permeability.

Table 1. Comparison of alternative mixture momentum equations

(i) Formulation developed by Prescott *et al.* [36]:

$$\frac{\partial}{\partial t}(\rho_m u_m)+\nabla\cdot(\rho_m \mathbf{V}_m u_m) = -g_l\frac{\partial p_l}{\partial x}-\frac{R_x}{g_l}(u_m-u_s) +g_l\rho_l B_x-\nabla\cdot\left[\left(\frac{\rho_m f_s}{f_l}\right)(\mathbf{V}_m-\mathbf{V}_s)(u_m-u_s)\right]+\frac{\partial}{\partial t}(g_s\rho_s u_s)+\nabla\cdot(g_s\rho_s\mathbf{V}_s u_s) +\nabla\cdot(\mu_l^*\nabla u_m)-\mu_l^*[u_s\nabla^2 f_s+2\nabla u_s\cdot\nabla f_s]. \quad (29)$$

(ii) Formulation developed from liquid momentum equation (model 1):

$$\frac{\partial}{\partial t}(\rho_m u_m)+\nabla\cdot(\rho_m \mathbf{V}_m u_m) = -g_l\frac{\partial p_l}{\partial x}-\frac{R_x\rho_m}{g_l\rho_l}(u_m-u_s)+u_{li}\Gamma_l +g_l\rho_l B_x-\nabla\cdot\left[\left(\frac{\rho_m f_s}{f_l}\right)(\mathbf{V}_m-\mathbf{V}_s)(u_m-u_s)\right]+\frac{\partial}{\partial t}(g_s\rho_s u_s)+\nabla\cdot(g_s\rho_s\mathbf{V}_s u_s) +\nabla\cdot\left(\mu_l^*\frac{\rho_m}{\rho_l}\nabla u_m\right)+\nabla\cdot\left[\mu_l^* u_m\nabla\left(\frac{\rho_m}{\rho_l}\right)\right]-\nabla\cdot\left(\mu_l^*\frac{\rho_m f_s}{\rho_l}\nabla u_s\right)-\nabla\cdot\left[\mu_l^* u_s\nabla\left(\frac{\rho_m f_s}{\rho_l}\right)\right]+\nabla\cdot[\mu_l^* u_{li}(\nabla g_s)]. \quad (20)$$

(iii) Formulation developed from superposition of the solid and liquid momentum equations (model 2):

for dispersed flow with moving equiaxed crystals

$$\frac{\partial}{\partial t}(\rho_m u_m)+\nabla\cdot(\rho_m \mathbf{V}_m u_m) = -\frac{\partial p}{\partial x}+\rho_m B_x-\nabla\cdot\left[\left(\frac{\rho_m f_s}{f_l}\right)(\mathbf{V}_m-\mathbf{V}_s)(u_m-u_s)\right] +\nabla\cdot\left(\mu_l^*\frac{\rho_m}{\rho_l}\nabla u_m\right)+\nabla\cdot\left[\mu_l^* u_m\nabla\left(\frac{\rho_m}{\rho_l}\right)\right]-\nabla\cdot\left(\mu_l^*\frac{\rho_m f_s}{\rho_l}\nabla u_s\right)-\nabla\cdot\left[\mu_l^* u_s\nabla\left(\frac{\rho_m f_s}{\rho_l}\right)\right] +\nabla\cdot[\mu_l^* u_{li}(\nabla g_s)]+\nabla\cdot[g_s\mu_s^*\nabla u_s] \quad (25)$$

for stationary columnar structure and packed equiaxed crystals or fragments

$$\frac{\partial}{\partial t}(\rho_m u_m)+\nabla\cdot(\rho_m \mathbf{V}_m u_m) = -g_l\frac{\partial p_l}{\partial x}-\frac{R_x\rho_m}{g_l\rho_l}u_m+u_{li}\Gamma_l+g_l\rho_l B_x -\nabla\cdot\left[\left(\frac{\rho_m f_s}{f_l}\right)\mathbf{V}_m u_m\right]+\nabla\cdot\left(\mu_l^*\frac{\rho_m}{\rho_l}\nabla u_m\right)+\nabla\cdot\left[\mu_l^* u_m\nabla\left(\frac{\rho_m}{\rho_l}\right)\right]+\nabla\cdot[\mu_l^* u_{li}(\nabla g_s)]. \quad (28)$$

In the x-coordinate direction of a Cartesian system, equation (27) can be written as

$$\frac{\partial}{\partial t}(\rho_m u_m)+\nabla\cdot(\rho_m \mathbf{V}_m u_m) = -g_l\frac{\partial p_l}{\partial x}-\frac{R_x\rho_m}{g_l\rho_l}u_m+u_{li}\Gamma_l+g_l\rho_l B_x-\nabla\cdot\left[\left(\frac{\rho_m f_s}{f_l}\right)\mathbf{V}_m u_m\right]+\nabla\cdot\left(\mu_l^*\frac{\rho_m}{\rho_l}\nabla u_m\right)+\nabla\cdot\left[\mu_l^* u_m\nabla\left(\frac{\rho_m}{\rho_l}\right)\right]+\nabla\cdot[\mu_l^* u_{li}(\nabla g_s)]. \quad (28)$$

2.2.3. *Comparison of alternative formulations of the mixture momentum equation.* Various formulations of the x-momentum equation for a solidification system are summarized in Table 1. Except for terms accounting for interfacial momentum transfer due to phase change and the contribution of interface motion to the liquid viscous stress [third and twelfth terms on the right-hand side of equation (20)], the first model, equation (20), is equivalent to that developed by Prescott *et al.* [36], equation (29) in Table 1, if the assumptions of Prescott *et al.* ($\rho_m/\rho_l = 1$, $\nabla^2 u_s = 0$, and constant μ_l^*) are applied to equation (20). Since the solid stress was modeled through the solid momentum equation in the derivation of equation (29), rather than through use of an additional constitutive equation, the final model equation of Prescott *et al.* [36] is actually the liquid momentum equation, but expressed in terms of the mixture velocity. Hence, it should be equivalent to model 1.

Since the mixture momentum equation for model 2 of this study is obtained by summing the liquid and solid momentum equations, the solid transport terms do not appear on the right-hand side of equation (28). However, in addition to terms associated with the macroscopic liquid viscous stress, a term associated with the macroscopic solid stress appears in the final result. However, for a dispersed flow with low g_s, the effective solid viscosity is approximately equal to the liquid viscosity [see equation (23)] and the sixth and ninth terms on the right-hand side of equation (25) cancel each other in the case of equivalent phase densities. In this case the solid viscous stress term does not appear in the final result.

For a dispersed flow with moving equiaxed crystals or fragments, pressure equilibrium eliminates all of

the interfacial momentum transfer terms through the interfacial momentum balance, and the effective solid stress is modeled in terms of a solid velocity gradient by treating the solid as pseudo-fluid. In both the first and second models, an additional solid transport equation is needed to account for crystal settling/floating and is developed in the companion paper [1].

For a stationary solid structure, the solid velocity is zero but the interfacial momentum transfer terms are retained in the final form of the momentum equation. Although it is not clear how to model the solid stress for a stationary solid, the term may be equated to zero if the solid is assumed to be rigid and deformation is neglected. With zero solid velocity and equivalent phase densities, equations (20), (28) and (29) yield equivalent results.

Preference for the model 1 or model 2 representation of the momentum equation is somewhat arbitrary and may depend upon the nature of solidification conditions. If, for example, the average solid and liquid velocities are comparable, the two phases may be said to be well mixed and model 2, which originates from mixture momentum considerations, may be preferred. If, however, liquid flow conditions are intense and of special interest, model 1, which originates from the liquid momentum equation, may be preferred.

Except for the model 2 version of the momentum equation for a dispersed flow, where pressure equilibrium is imposed, the pressure gradient term in the other forms of the momentum equation includes the liquid volume fraction. Prescott *et al.* [36] converted this term to a standard form by utilizing a version of Darcy's law which included the pressure gradient, buoyancy force, and Darcy damping terms. This transformation is only valid for stationary solids with negligible inertia effects. However, the pressure gradient term may be expressed as

$$-g_l\nabla p_l = -\nabla p_l + g_s\nabla p_l \tag{30}$$

which is a form better suited for CFD. If the solid fraction is small, the last term is negligible and the equation reduces to that for pressure equilibrium in a dispersed flow.

2.3. *Energy conservation*

In the solidification of metal alloys, conditions may be influenced by solutal and thermal undercooling, and generally such effects should be included in a process model. However, since the Lewis number of a liquid metal is large ($Le \gtrsim 1000$), thermal equilibrium is readily maintained and nonequilibrium effects are more strongly influenced by solutal undercooling. Assuming thermal equilibrium to exist interfacially and volumetrically, $T_{li} = T_{si} = T_l = T_s = T$, the requirement of energy conservation may be expressed in terms of the mixture equation used in the continuum solidification model [12], which is of the form

$$\begin{aligned}
&\frac{\partial}{\partial t}(\rho_m h_m) + \nabla\cdot(\rho_m h_m \mathbf{V}_m) \\
&= \nabla\cdot(\mathbf{k}_m\nabla T) - \nabla\cdot[\rho_m(h_l - h_m)(\mathbf{V}_m - \mathbf{V}_s)] \\
&= \nabla\cdot\left(\frac{\mathbf{k}_m}{c_{ps}}\nabla h_m\right) + \nabla\cdot\left[\frac{\mathbf{k}_m}{c_{ps}}\nabla(h_s - h_m)\right] \\
&\quad -\nabla\cdot[\rho_m(h_l - h_m)(\mathbf{V}_m - \mathbf{V}_s)].
\end{aligned} \tag{31}$$

This equation can also be obtained by summing enegy conservation equations for the solid and liquid phases [23] and using an interfacial energy balance. The mixture enthalpy and thermal conductivity tensor are defined, respectively, as $h_m = f_l h_l + f_s h_s$ and $\mathbf{k}_m = g_l\mathbf{k}_l^* + g_s\mathbf{k}_s^*$. The effective macroscopic thermal conductivities, $\mathbf{k}_l^*$ and $\mathbf{k}_s^*$, account for the presence of the solid phase and a dispersive flux (such as a turbulent heat flux) [23]. In general, the macroscopic thermal conductivities are different from their microscopic counterparts. However, little research has been performed on this issue, and the macroscopic thermal conductivities are typically equated to the microscopic quantities.

The liquid and solid enthalpies are related to the equilibrium temperature through the following thermodynamic relations:

$$h_l = c_{pl}T + h^0 \quad \text{and} \quad h_s = c_{ps}T \tag{32}$$

where h^0 is the reference enthalpy, given by $(c_{ps} - c_{pl})T_e + L$, and L is the latent heat of fusion at the eutectic temperature. In deriving equation (31), the temperature gradient has been expressed in terms of the solid enthalpy by using equation (32) with the definition of the mixture enthalpy.

Once the mixture enthalpy is known, the equilibrium temperature may be determined from the expression

$$T = \frac{h_m - f_l h^0}{c_{pm}} \tag{33}$$

and the enthalpies of the liquid and solid phases can then be determined from equation (32). The mixture specific heat c_{pm} is defined as $f_l c_{pl} + f_s c_{ps}$. During the eutectic reaction ($T = T_e$), the mixture enthalpy can alternatively be used to determine the solid mass fraction and details are presented in Section 2.5.

2.4. *Species conservation*

The species mixture conservation equation can be obtained by summing the species conservation equations of the solid and liquid phases [23] to yield

$$\begin{aligned}
&\frac{\partial}{\partial t}(\rho_m f_m^\alpha) + \nabla\cdot(\rho_m f_m^\alpha \mathbf{V}_m) \\
&= \nabla\cdot(\rho_m f_l D_l^*\nabla f_l^\alpha) - \nabla \\
&\quad\cdot[\rho_m(\mathbf{V}_m - \mathbf{V}_s)(f_l^\alpha - f_m^\alpha)] + \nabla\cdot(\rho_m f_s D_s^*\nabla f_s^\alpha) \\
&= \nabla\cdot(\rho_m D_m\nabla f_m^\alpha) + \nabla\cdot(\rho_m f_l D_l^*\nabla(f_l^\alpha - f_m^\alpha) \\
&\quad -\nabla\cdot[\rho_m(\mathbf{V}_m - \mathbf{V}_s)(f_l^\alpha - f_m^\alpha)] \\
&\quad +\nabla\cdot(\rho_m f_s D_s^*\nabla(f_s^\alpha - f_m^\alpha)
\end{aligned} \tag{34}$$

where f_m^α and D_m are the mixture species concentration and effective macroscopic species diffusivity, defined as $f_m^\alpha = f_l f_l^\alpha + f_s f_s^\alpha$ and $D_m = f_l D_l^* + f_s D_s^*$, respectively. The effective macroscopic species diffusivities of the liquid and solid phases, D_l^* and D_s^*, account for existence of the solid phase and a solutal dispersive flux [23]. Without definitive knowledge of these quantities, however, the macroscopic species diffusivities are simply equated to the microscopic quantities. Typically, diffusion in the solid is negligible and the mixture species diffusivity D_m reduces to $f_l D_l^*$. Equation (34) is then identical to the mixture species equation developed by Bennon and Incropera [12].

In the traditional mixture continuum model, nonequilibrium effects due to solutal undercooling are not considered, and species concentrations in the solid and liquid phases are obtained from the phase diagram and the lever rule. Other assumptions implicit in this model include equivalent interfacial and average species concentrations for the solid and liquid, thermal equilibrium, no solid movement, and negligible density differences in the solid and liquid phases. As well as allowing for solid motion, assumptions which should be relaxed relate to the inclusion of nonequilibrium effects due to solutal undercooling of the liquid and liquid interfacial species transfer. These considerations are discussed in the following sections.

2.5. *Solid mass fraction and phase compositions*

In the continuum solidification model, the solid mass fraction f_s is indirectly determined from supplemental relations (thermodynamic and phase diagram relations) and not directly by computing the interfacial mass transfer rate, Γ_s, as in the two-phase model [27]. The solid volume fraction g_s and the phase change rate Γ_s are related to each other through the solid mass conservation requirement, equation (2). For a general (primary or off-eutectic) solidification process, the solid mass fraction may be calculated from knowledge of the mixture species concentration (obtained from the species conservation equation) and the interfacial species concentrations of the solid and liquid phases, which are related to the equilibrium temperature through the phase diagram. For a eutectic reaction, it may be necessary to consider coexisting α and β solid phases, as well as a liquid phase [41]. For simplicity, however, the reaction may be treated as isothermal and interfacial species concentrations of the solid (α and/or β) and liquid phases may be equated, thereby eliminating interfacial species transport. In this case, the solid mass fraction must be obtained from the mixture enthalpy and hence by solving the mixture energy equation. Therefore, for the general (off-eutectic) and special (eutectic) reactions, the solid mass fraction and the solid and liquid species concentrations are calculated from separate procedures. When the mixture temperature exceeds the liquidus temperature ($T \geqslant T_{ld}$, or $h_m \geqslant h_{ld}$), solidification does not occur and temperature is calculated from equation (33) with $f_l = 1$. The liquidus temperature is calculated from the phase diagram (see Fig. 2), and the enthalpy associated with the liquidus temperature is calculated from equation (32). For example, for a binary alloy of initial composition f_0^α less than the eutectic composition f_e^α, the liquidus temperature and enthalpy can be expressed as

$$T_{ld} = T_m^\alpha + \left(\frac{T_e - T_m^\alpha}{f_e^\alpha}\right) f_m^\alpha \quad \text{and} \quad h_{ld} = c_{pl} T_{ld} + h^0. \tag{35}$$

2.5.1. *General (off-eutectic) solidification.* When the melt is cooled to a temperature below the liquidus temperature, solidification occurs over a range of temperatures ($T_e \leqslant T \leqslant T_{ld}$) and enthalpies ($h_e \leqslant h_m \leqslant h_{ld}$), where h_e is the enthalpy associated with a two-phase mixture of primary solid and liquid at the eutectic temperature. From the definition of the mixture species concentration, the solid mass fraction may be expressed as

$$f_s = \frac{f_m^\alpha - f_l^\alpha}{f_s^\alpha - f_l^\alpha}. \tag{36}$$

If the solid and liquid phases are assumed to be well-mixed, it follows that

$$f_l^\alpha = f_{li}^\alpha \tag{37}$$

and

$$f_s^\alpha = f_{si}^\alpha \tag{38}$$

and consideration of nonequilibrium effects due to solutal undercooling is precluded. Solid and liquid phase concentrations can then be determined by using relations based on characteristics of the equilibrium phase diagram ($T_e, f_e^\alpha, \kappa_p$, and T_m^α), shown in Fig. 2, with knowledge of the equilibrium temperature T.

If diffusion in the solid is considered, the volume-averaged solid species concentration is not equal to the interfacial solid species concentration and may be expressed as

$$f_s^\alpha = f_{si}^\alpha - \Delta f_s^\alpha \tag{39}$$

where the difference Δf_s^α depends on species diffusion in the solid, crystal or dendrite growth rate, interfacial geometry, and solid structure. Modeling of microscale finite rate solutal diffusion in the solid is essential to predicting microsegregation. Ohnaka [44], for example, has used the assumption of parabolic concentration profiles in individual dendrites to obtain predictions of microsegregation, which are in good agreement with experimental results. By representing the dendritic structure in terms of simple geometries (planar, cylindrical, or spherical), the volume averaged solid species concentration can be obtained in terms of the interfacial concentration, mass diffusivity, and structure of the solid, including its characteristic length. The analysis involves integrating the solute concentration over the microscopic scale associated with the control volume. However, under conditions for which macroscopic transport is significant, micro-

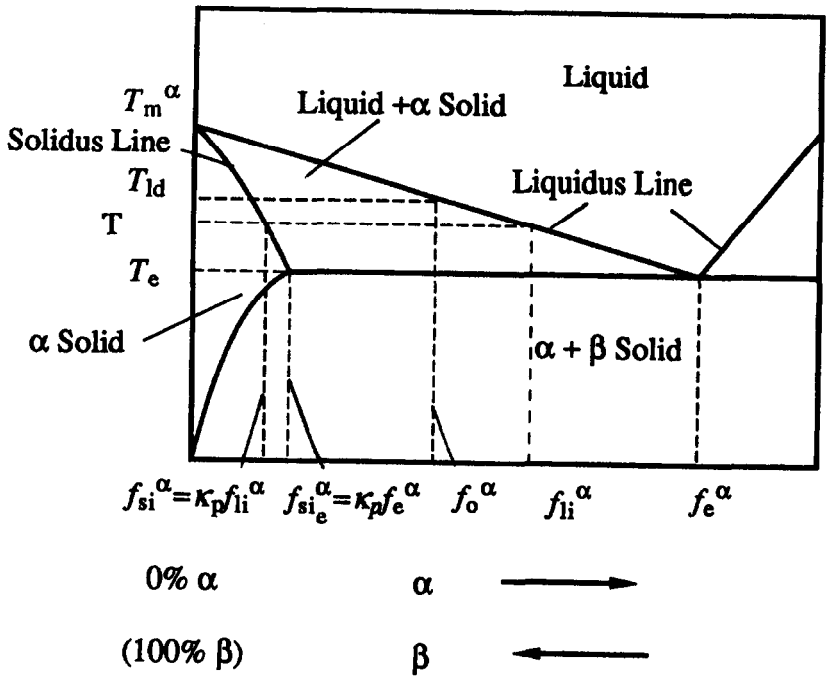

Fig. 2. Typical equilibrium phase diagram for a binary alloy system (α–β).

segregation effects may often be neglected and equation (38) used as a first approximation.

In a real crystal or dendrite growth process, diffusion in the liquid is not complete and there is accumulation of solute at the liquid side of the interface, as well as in a boundary layer adjoining the interface. The assumption of a well-mixed solute in the liquid (the lever rule) is inconsistent with the existence of nonequilibrium due to solutal undercooling, precluding substitution of the interfacial liquid species concentration for the volume averaged liquid species concentration. Hence, similar to equation (39), the liquid species concentration can be expressed as

$$f_l^\alpha = f_{li}^\alpha - \Delta f_l^\alpha \tag{40}$$

where Δf_l^α is the solutal undercooling, which accounts for the difference between the interfacial and volume averaged liquid species concentrations. Hence, through development of an appropriate model for Δf_l^α, nonequilibrium effects due to solutal undercooling may be considered. Such a model is discussed in the companion paper [1].

The interfacial liquid and solid species concentrations, f_{li}^α and f_{si}^α, may be related to the equilibrium temperature through relations inferred from the equilibrium phase diagram (see Fig. 2). For example, for a binary alloy of initial composition f_0^α less than the eutectic composition, one has

$$f_{li}^\alpha = \frac{T - T_m^\alpha}{T_e - T_m^\alpha} f_e^\alpha \quad \text{and} \quad f_{si}^\alpha = \kappa_p f_{li}^\alpha \tag{41}$$

where the liquidus and solidus lines have been linearized.

Once the interfacial concentrations, f_{li}^α and f_{si}^α, and the concentration differences, Δf_l^α and Δf_s^α, are determined, equation (36) can be used to obtain the solid mass fraction by substituting for the average species concentrations of the solid and liquid phases from equations (39) and (40), and for the mixture species concentration determined from the mixture conservation equation, equation (34). A numerical iteration procedure would be used to compute the solid mass fraction and to thereby account for solutal nonequilibrium effects.

The enthalpy associated with a two-phase mixture of primary solid and liquid at the eutectic temperature can be expressed as [18]

$$h_e = (1 - f_{se})(c_{pl} T_e + h^0) + f_{se} c_{ps} T_e = c_{ps} T_e + (1 - f_{se}) L \tag{42}$$

where the solid mass fraction at the onset of a eutectic reaction, f_{se}, can be calculated from equation (36)

$$f_{se} = \frac{f_m^\alpha - f_e^\alpha}{f_{si_e}^\alpha - f_e^\alpha}. \tag{43}$$

The solubility limit of the solid phase $f_{si_e}^\alpha$ can also be obtained from the phase diagram (Fig. 2). For a binary mixture of Al–Cu or Pb–Sn, it can be expressed as $\kappa_p f_e^\alpha$, while for a binary mixture of NH_4Cl–H_2O it is zero. If $f_m^\alpha \leqslant f_{si_e}^\alpha$, there is no eutectic reaction and liquid is solidified to the α solid phase. In this case, $f_s = 1$ when $T \leqslant T_{sd} = T_m^\alpha + [(T_e - T_m^\alpha)/\kappa_p f_e] f_m^\alpha$, where T_m^α is the melting point of the pure species α.

2.5.2. *Eutectic reaction.* For a eutectic reaction, the

temperature and the interfacial species concentrations of the solid and liquid phases are

$$T = T_e \quad \text{and} \quad f_{li}^{\alpha} = f_{si}^{\alpha} = f_e^{\alpha}. \tag{44}$$

During a eutectic reaction, the mixture enthalpy decreases from h_e to $h_{sol}(= c_{ps}T_e)$. Since the liquid and interfacial liquid compositions are well mixed, solutal undercooling is negligible and the volume averaged liquid and solid concentrations can be expressed as

$$f_l^{\alpha} = f_{li}^{\alpha} = f_e^{\alpha} \quad \text{and} \quad f_s^{\alpha} = \frac{f_m^{\alpha} - f_l f_l^{\alpha}}{f_s}. \tag{45}$$

Since the temperature is known, the definition of the mixture enthalpy can be used to calculate the solid mass fraction from the following expression:

$$f_s = 1 - (1 - f_{se})\frac{h_m - c_{ps}T_e}{h_e - c_{ps}T_e} = 1 - \frac{h_m - c_{ps}T_e}{L}. \tag{46}$$

CONCLUSIONS

Existing continuum and two-phase models for solidification of binary mixtures are assessed in terms of advantages and shortcomings, and a new model is proposed which retains the operational convenience of the continuum model, while allowing for the inclusion of important features of the two-phase model. Several assumptions inherent in the original formulation of the continuum model are relaxed, making it possible to account for the effects of solutal undercooling, solidification shrinkage, and solid movement.

The model consists of a set of macroscopic continuum equations governing the conservation of mass, momentum, energy, and species in a binary mixture. They are equations (3), (19), (31) and (34) and are expressed in terms of the mixture density ρ_m, velocity $\mathbf{V}_m$, enthalpy h_m, and species concentration f_m^{α}. The formulation of the mixture momentum equation expressed by equation (19) is preferred because of its applicability to both dispersed and stationary solid phases and because of the numerical convenience it affords. Constitutive equations for the viscous stress and the thermal and mass diffusive fluxes have been included in the model equations, and supplemental relations are provided to compute the requisite phase interaction quantities. Enthalpies of the solid and liquid phases can be calculated from thermodynamic relations, equations (32), and the species concentrations of the solid and liquid phases can be obtained from equations (39) and (40), where consideration is given to interfacial species variables and solutal undercooling. The interfacial momentum transfer term due to interactions between the liquid and solid phases is modeled in terms of a drag coefficient for the movement of equiaxed crystals in the melt [equation (15)] or a permeability tensor for flow through a continuous solid structure [equation (18)]. The interfacial species concentrations of the solid and liquid phases are determined from phase diagram relations as, for example, from equation (41). During off-eutectic solidification, the solid mass fraction is calculated from an equilibrium model, equation (36), and the equilibrium temperature is determined from equation (33). For a eutectic reaction at which the temperature is known, the solid mass fraction is calculated from equation (46).

To complete the model development, it is necessary to establish relations between solid and liquid velocity components under conditions involving solid movement and to develop models for solutal undercooling and the rate of the crystal nucleation. Such models are linked to microscopic features of solidification and provided by Ni and Incropera [1].

Acknowledgements—Support of this work has been provided by the U.S. Department of Energy under Award Number DE-FG02-87ER13759. We wish to thank Dr P. J. Prescott and Mr M. J. M. Krane for reviewing the manuscript and for their many helpful comments and criticisms.

REFERENCES

1. J. Ni and F. P. Incropera, Extension of the continuum model for transport phenomena occurring during metal alloy solidification—II. Microscopic considerations, *Int. J. Heat Mass Transfer* **38,** 1285–1296 (1995).
2. M. C. Flemings, *Solidification Processing*. McGraw-Hill, New York (1974).
3. W. Kurz and D. J. Fisher, *Fundamentals of Solidification*. Trans. Tech. Publications, Adermannsdorf (1989).
4. M. C. Flemings, Solidification processing. In *Materials Science and Technology* (Edited by R. W. Cahn, P. Hassen and E. J. Kramer), Vol. 15, pp. 1–56. VCH, New York (1991).
5. R. S. Steube and A. Hellawell, An alternative approach to modeling the grain structure of castings. In *Micro-Macro Scale Phenomena in Solidification* (Edited by C. Beckermann, L. A. Bertram, S. J. Pien and R. E. Smelser), HTD-Vol. 218/AMD-Vol. 139, pp. 73–82. ASME, New York (1992).
6. M. Rappaz, Modelling of microstructure formation in solidification processes, *Int. Mater. Rev.* **34**(3), 93–123 (1989).
7. R. Viskanta, Mathematical modeling of transport processes during solidification of binary systems, *JSME Int. J. Ser.* II **33**(3), 409–423 (1990).
8. C. Beckermann and R. Viskanta, Mathematical modeling of transport phenomena during alloy solidification, *Appl. Mech. Rev.* **46**(1), 1–27 (1993).
9. P. J. Prescott and F. P. Incropera, Binary solid–liquid phase change with fluid flow. In *Advances in Transport Processing* (Edited by A. S. Mujumdar and R. A. Mashelkar), Vol. IX, pp. 57–101. Elsevier Science, Amsterdam (1993).
10. R. N. Hills, D. E. Loper and P. H. Roberts, A thermodynamically consistent model of a mushy zone, *Q. J. Mech. Appl. Math.* **36,** 505–536 (1983).
11. V. C. Prantil and P. R. Dawson, Application of a mixture theory to continuous casting. In *Transport Phenomena in Materials Processing* (Edited by M. M. Chen, J. Mazumder and C. L. Tucker III), pp. 469–484. ASME, New York (1983).
12. W. D. Bennon and F. P. Incropera, A continuum model for momentum, heat and species transport in binary solid–liquid phase change systems—I. Model formulation, *Int. J. Heat Mass Transfer* **30,** 2161–2170 (1987).
13. V. R. Voller and C. Prakash, A fixed grid numerical modelling methodology for convection–diffusion mushy

region phase-change problems, *Int. J. Heat Mass Transfer* **30,** 1709–1719 (1987).
14. V. R. Voller, A. D. Brent and C. Prakash, The modelling of heat, mass, and solute transport in solidification systems, *Int. J. Heat Mass Transfer* **32,** 1719–1731 (1989).
15. W. D. Bennon and F. P. Incropera, Numerical analysis of binary solid–liquid phase change using a continuum model, *Numer. Heat Transfer* **13,** 277–296 (1988).
16. W. D. Bennon and F. P. Incropera, A continuum model for momentum, heat and species transport in binary solid–liquid phase change systems—II. Application to solidification in a rectangular cavity, *Int. J. Heat Mass Transfer* **30,** 2171–2187 (1987).
17. D. G. Neilson and F. P. Incropera, Unidirectional solidification of a binary alloy and the effects of induced fluid motion, *Int. J. Heat Mass Transfer* **34,** 1717–1732 (1991).
18. P. J. Prescott and F. P. Incropera, Numerical simulation of a solidifying Pb–Sn alloy: the effects of cooling rate on thermosolutal convection and macrosegregation, *Metall. Trans. B* **22B,** 529–540 (1991).
19. K. C. Chiang and H. L. Tsai, Shrinkage-induced fluid flow and domain change in two-dimensional alloy solidification, *Int. J. Heat Mass Transfer* **35,** 1763–1770 (1992).
20. C. Beckermann and R. Viskanta, Double-diffusive convection during dendritic solidification of a binary mixture, *Physicochem. Hydraul.* **10,** 195–213 (1988).
21. S. Ganesan and D. R. Poirier, Conservation of mass and momentum for the flow of interdendritic liquid during solidification, *Metall. Trans. B.* **21B,** 173–181 (1990).
22. J. Ni and C. Beckermann, A two-phase model for mass, momentum, heat, and species transport during solidification. In *Transport Phenomena in Material Processing* (Edited by M. Charmchi, M. K. Chyu, Y. Joshi and S. M. Walsh), HTD-Vol. 132, pp. 45–56. ASME, New York (1990).
23. J. Ni and C. Beckermann, A volume-averaged two-phase model for transport phenomena during solidification, *Metall. Trans. B* **22B,** 349–361 (1991).
24. R. J. Feller and C. Beckermann, Modeling of the globulitic solidification of a binary metal alloy, *Int. Commun. Heat Mass Transfer* **20,** 311–322 (1993).
25. M. C. Schneider, Modeling the columnar dendritic solidification of lead–tin alloys, M.S.M.E. Thesis, The University of Iowa (1991).
26. C. Beckermann and J. Ni, Modeling of equiaxed solidification with convection. In *First International Conference on Transport Phenomena in Processing* (Edited by S. I. Guceri), pp. 308–317. Technomic, Lancaster, PA (1993).
27. J. Ni and C. Beckermann, Modeling of globulitic alloy solidification with convection, *J. Mater. Process. Mater. Sci.* **2**(2), 217–231 (1993).
28. M. C. Flemings and G. E. Nereo, Macrosegregation: Part I, *TMS-AIME* **239,** 1449–1461 (1967).
29. M. C. Flemings, R. Mehrabian and G. E. Nereo, Macrosegregation: Part II, *TMS-AIME* **242,** 41–49 (1968).
30. M. C. Flemings and G. E. Nereo, Macrosegregation: Part III, *TMS-AIME* **242,** 50–55 (1968).
31. R. Mehrabian, M. Keane and M. C. Flemings, Interdendritic fluid flow and macrosegregation: influence of gravity, *Metall. Trans.* **1,** 1209–1220 (1970).
32. S. Kou, D. R. Poirier and M. C. Flemings, Macrosegregation in rotated remelted ingots, *Metall. Trans. B* **9B,** 711–719 (1978).
33. T. Fujii, D. R. Poirier and M. C. Flemings, Macrosegregation in a multicomponent low alloy steel, *Metall. Trans. B* **10B,** 331–339 (1979).
34. S. D. Ridder, S. Kou and R. Mehrabian, Effect of fluid flow on macrosegregation in axisymmetric ingots, *Metall. Trans. B* **12B,** 435–447 (1981).
35. M. Hassanizadeh and W. G. Gray, General conservation equations for multi-phase systems: constitutive theory for porous media flow, *Adv. Water Resources* **3,** 25–40 (1980).
36. P. J. Prescott, F. P. Incropera and W. D. Bennon, Modeling of dendritic solidification systems: reassessment of the continuum momentum equation, *Int. J. Heat Mass Transfer* **34,** 2351–2359 (1991).
37. V. R. Voller, Effect of solidification morphology on the macroscopic behaviour of solidification systems, presented at *NATO Advanced Research Workshop*, 7–14 March (1992).
38. M. Ishii, *Thermo-fluid Dynamics Theory of Two-phase Flow*. Eyrolles, Paris (1975).
39. M. Ishii and N. Zuber, Drag coefficient and relative velocity in bubble, droplet or particulate flows, *A.I.Ch.E. Jl* **25,** 843–855 (1979).
40. D. R. Poirier, Permeability for flow of interdendritic liquid in columnar-dendritic alloys, *Metall. Trans. B* **18B,** 245–255 (1987).
41. M. C. Schneider and C. Beckermann, A numerical study of the combined effects of microsegregation, mushy zone permeability, and contraction driven flow on macrosegregation and eutectic formation in binary alloy solidification, ASME Winter Annual Meeting, Chicago (1994).
42. J. Ding and D. Gidaspow, A bubble fluidization model using kinetic theory of granular flow, *A.I.Ch.E. Jl* **36,** 523–538 (1990).
43. D. A. Drew, Mathematical modeling of two-phase flow, *A. Rev. Fluid Mech.* **15,** 261–291 (1983).
44. I. Ohnaka, Mathematical analysis of solute redistribution during solidification with diffusion, *Iron Steel Inst. Jap.* **26**(12), 1045–255 (1986).